Theoretical investigation of electron-phonon interaction in the orthorhombic phase of Mo_2C

E. Karaca[a,b], S. Bağcı[b], H. M. Tütüncü[a,b], H.Y. Uzunok[a,b] and G. P. Srivastava[c]

[a] *Sakarya Üniversitesi, BIMAYAM, Biyomedikal, Manyetik ve Yarıiletken Malzemeler Araştırma Merkezi, 54187, Sakarya , Turkey*

[b] *Sakarya Üniversitesi, Fen-Edebiyat Fakültesi, Fizik Bölümü, 54187, Adapazarı, Turkey*

[c] *School of Physics, University of Exeter, Stocker Road, Exeter EX4 4QL, UK*

Abstract

We have studied the structural, electronic, elastic, mechanical, vibrational and electron-phonon interaction properties of Mo_2C crystallizing in the simple orthorhombic ζ-Fe_2N-type crystal structure by using the generalized gradient approximation of the density functional theory and the plane wave *ab initio* pseudopotential method. A critical assessment of the calculated electronic structure and density of states reveals that the bonding in in this material is a combination of covalent, ionic and metallic in nature. The calculated values of the second order elastic constants signal its mechanical stability. An examination of the calculated Eliashberg spectral function reveals that Mo-related phonon modes couple strongly to electrons due to the significant presence of Mo d electrons at the Fermi energy. From the integration of this spectral function, the value of average electron-phonon coupling parameter is determined to be of the intermediate strength 0.709. Finally, the value of the superconducting critical temperature is calculated to be 7.37 K, in excellent accordance with its measured value of 7.30 K.

Key words: A. transition metal alloys and compounds, superconductors; C. elasticity, electronic properties, phonons, electron-phonon interactions; D. computer simulations

[1] Corresponding Author: H. M. Tütüncü Tel: +90 264 295 60 72 Fax: +90 264 295 59 50 e-Mail: tutuncu@sakarya.edu.tr

1 Introduction

The transition metal carbides, displaying matchless physical and chemical properties such as good chemical stabilities, high melting points, remarkable electrical and thermal conductivities, extreme hardness, excellent corrosion and wear resistance [1–5], have received a great deal of interest as useful materials for cutting tools and hard-coatings [5–11]. One of the most important transition metal carbide, molybdenum semi-carbide (Mo_2C), has been largely applied in steel and in metal ceramics [12]. Mo_2C adopts both orthorhombic and hexagonal crystalline solids [13–18]. The orthorhombic phase has been experimentally [19,20] found to be more stable than the hexagonal phase. In addition, the orthorhombic phase of Mo_2C is reported to exhibit superconductivity at 7.30 K [21]. Moreover, Mo_2C is known to exhibit hydogen-related catalytic activities like noble metals such as hydrogenation, dehydrogenation, hydrogenolysis, methanation, aromatization, hydrocracking, hydrodesulfurization, hydrodenitrogenation, and hydrogen production from reforming of oxygenated compounds [22–38]. The orthorhombic phase of Mo_2C has also been reported as an active catalytic phase for the watergas shift (WGS) reaction [39–41] and also as a highly useful backing to support to Pt nanoparticles in the catalyzed WGS reaction [42]. In addition, the orthorhombic Mo_2C has been discovered to catalytically turn benzene into cyclohexane in a highly influential manner [43]. Above all, steam reforming catalysis has been realized using the orthorhombic phase of Mo_2C [44].

Pulse-echo measurements of ultrasonic wave velocity [45] have been utilized to obtain the elastic stiffness moduli and related elastic properties of ceramic samples of orthorhombic Mo_2C as functions of temperature in the range 130-295 K and hydrostatic pressure up to 0.2 GPa at room temperature. This experimental work [45] reveals that the orthorhombic Mo_2C ceramic is a relatively rigid material elastically: the longitudinal elastic stiffness and the adiabatic bulk modulus of this material is high. Furthermore, they grow with diminishing temperature and exhibit a knee [Huesyin, is 'knee' the right word here?] at about 200 K, below which longitudinal acoustic mode softening is present.

The unique physical and chemical properties of Mo_2C have motivated theoreticians to investigate its structural, elastic, mechanical, electronic and vibrational properties. A large number of theoretical works [20,46–57] exist on its physical properties. *Ab inito* pseudopotential calculations [20] within the local density approximation (LDA) made on both phases of Mo_2C have indicated that the orthorhombic phase is slightly lower in energy that the hexagonal one. In this theoretical work [20], the calculated charge distribution clearly suggests a existence for directional Mo-C bonding. Following this theoretical work, first-principles full-potential muffin-tin orbital calculations [46] were conducted in order to investigate structural and electronic properties of hexagonal and orthorhombic Mo_2C. This theoretical work also confirms that the orthorhombic phase is more stable than hexagonal one. In 2009, Wang and co-workers [49] determined the lattice parameters, elastic constant matrices and overlap population for both phases in order to understand the characterization of the hardness and melting point of both structures using the first-principles plane wave pseudopotential method based on the density functional theory within the generalized gradient approximation (GGA). Their electronic results reveal that the hybridization effect between Mo d and C p states in the orthorhombic phase is considerably stronger than that in the hexagonal one. Following this theoretical work, the *ab-inito* pseudopotential method [50] was also used to study structural, electronic and elastic

properties of the orthorhombic and hexagonal Mo_2C. The obtained elastic results [50] for both phases indicate that they are both mechanically stable. Furthermore, the obtained results for the enthalpy of these structures reveal that the orthorhombic phase can form more easily compared to the hexagonal one. Finally, the electronic results of this theoretical work [50] suggest that bonding in both phases of Mo_2C contains a mixture of covalent and metallic character. Density functional theory calculations within GGA [52] were made to examine the electronic structures and formation energies of semi-carbides M_2C and sub-carbides M_4C (where M =V, Cr, Nb, Mo, Ta and W). The results from this theoretical [52] work indicate that M_2C carbide is more stable than M_4C. The GGA method was also used to probe the structural and electronic properties of catalytically relevant molybdenum carbide phases (cubic MoC, hexagonal MoC and orthorhombic Mo_2C) by Politi and co-workers [53]. This theoretical work deduces that the orthorhombic Mo_2C exhibits a stronger metallic character than the other two polymorphs. In 2016, Connetable [57] studied the structural, elastic, mechanical and vibrational properties of orthorhombic Mo_2C using the GGA method. This theoretical study [57] reveals that the orthorhombic phase of Mo_2C is dynamically stable.

In spite of considerable theoretical progress made in analyzing the structural, electronic, elastic and mechanical properties of orthorhombic Mo_2C, no theoretical works have been conducted to examine its electron-phonon interaction properties. A number of important physical properties of metals are controlled by electron-phonon interaction. In general, for any material, electrical and thermal resistivities, superconductivity, softening of phonon modes, renormalization of the low-temperature electronic component of the heat capacity, and a number of other physical phenomena can be commented obviously only with the knowledge of the spectral distribution function of the electron-phonon interaction. With this in mind, we have decided to investigate the structural, electronic, elastic, mechanical, vibrational and electron-phonon interaction properties of orthorhombic Mo_2C, with particular attention to the origin of superconductivity. We examine the structural and electronic properties by using the GGA method of density functional theory [58,59]. The electronic band structure and density of states near the Fermi energy are examined and discussed in detail. The influential stress-strain method [60] has been utilized in estimating the second order constants and the obtained results signal the mechanical stability of Mo_2C in its orthorhombic ζ-Fe_2N-type crystal structure. Then, the calculated values of second order elastic constants allow us to determine the polycrystalline bulk modulus (B), shear modulus (G), Young's modulus (E) and Poisson's ratio (σ) using the Voigt-Reuss-Hill (VHR) approach [61–63]. The calculated values of above physical quantities coincide with previous experimental and theoretical results [45,50,55,57]. We have conducted *ab initio* linear response calculations [58,59] of phonon dispersion curves and phonon density of states for orthorhombic Mo_2C. The calculated phonon spectrum confirms the dynamical stability of Mo_2C in its orthorhombic ζ-Fe_2N-type crystal structure. The electron-phonon matrix elements for orthorhombic Mo_2C have been evaluated by utilizing the linear response method [58,59] and the Migdal-Eliashbergh approach [64,65]. Then, our phonon results and electron-phonon matrix elements have been used to derive the Eliashbergh spectral function of orthorhombic Mo_2C which allows us to determine the electron-phonon coupling parameter and the logarithmic average of phonon frequency. Using the calculated values of above two physical quantities, the value of superconducting transition temperature is found to be 7.37 K which is in excellent agreement with its experimentally reported value of 7.30 K [21]. [Huseyin, the text in this paragrph should not be described in the Introduction section. You seem to do this in all papers, and I keep trying to indicate not to do that (or atleast reduce it). Please decide if you would like to leave this

paragraph as it is].

2 Method

We have conducted first principles calculations based on the pseudopotential method within the density functional theory using the Quantum-Espresso (QE) computer package [58,59]. The electron-ion interaction is taken into account by using norm-conserving pseudopotentials [66] while the exchange-correlation energy is evaluated by using the generalized gradient approximation (GGA) within the Perdew-Burke-Ernzerhof (PBE) approach [67]. The electronic wave functions are expanded in plane waves up to a maximal cutoff energy of 60 Ry. The orthorhombic crystal structure of Mo_2C is totally relaxed by employing the Broyden-Fletcher-Goldfrab-Shanno optimized method [68]. Self-consistent solutions to the Kohn-Sham equations [69] are obtained by employing a set of special $\boldsymbol{k}$ points generated by using the Monkhorst-Pack scheme [70]. For the Brillouin zone sampling, in the calculation of structural properties, a (8×8×8) Monkhorst-Pack $\boldsymbol{k}$ mesh is chosen, but for the band structure calculation a (24×24×24) Monkhorst-Pack $\boldsymbol{k}$ mesh is utilized. Phonon calculations have been realized by using the linear response approach based on the density functional theory [58,59]. We have computed eight dynamical matrices which correspond to a 2×2×2 $\boldsymbol{q}$-point mesh within irreducible segment of the Brillouin zone. Then, three dimensional Fourier interpolation has been made to obtain phonons for any desired $\boldsymbol{q}$ point.

Our electron-phonon interaction calculations have been made using the Migdal-Eliashberg theory and linear-response theory together [58,59,64,65]. The key quantities of the Migdal-Eliashberg theory [64,65], determined using the linear-response theory [58,59], are the electron-phonon matrix elements which possess the following form:

$$g^{\boldsymbol{q}j}_{(\boldsymbol{k}+q)m;\boldsymbol{k}n} = \sqrt{\frac{\hbar}{2M\omega_{\boldsymbol{q}j}}} < j, \boldsymbol{k}+qm|\Delta V^{SCF}_{\boldsymbol{q}}|i, \boldsymbol{k}n >, \tag{1}$$

where M is atomic mass and $\Delta V^{SCF}_{\boldsymbol{q}}$ refers to the derivative of the self-consistent effective potential with respect to the atomic displacements caused by a phonon with wave vector $\boldsymbol{q}$. The electron-phonon matrix elements allow us to calculate the the phonon linewidth $\gamma_{\boldsymbol{q}j}$,

$$\gamma_{\mathbf{q}j} = 2\pi\omega_{\mathbf{q}j} \sum_{\mathbf{k}nm} |\mathrm{g}^{\mathbf{q}j}_{(\mathbf{k}+\mathbf{q})m;\mathbf{k}n}|^2 \delta(\varepsilon_{\mathbf{k}n} - \varepsilon_F)\delta(\varepsilon_{(\mathbf{k}+\mathbf{q})m} - \varepsilon_F), \tag{2}$$

where $\omega_{\boldsymbol{q}j}$ and $\varepsilon_{(\mathbf{k}+\mathbf{q})m}$ refer to the phonon frequency and the energies of bands respectively. The electronic density of states, the phonon density of states, and the electron-phonon matrix elements are used to derive the Eliashberg function $\alpha^2F(\omega)$

$$\alpha^2F(\omega) = \frac{1}{2\pi N(E_F)} \sum_{\mathbf{q}j} \frac{\gamma_{\mathbf{q}j}}{\hbar\omega_{\mathbf{q}j}} \delta\left(\omega - \omega_{\mathbf{q}j}\right). \tag{3}$$

Here $N(E_F)$ depicts the electronic density of states at the Fermi level. Then, the average

electron-phonon coupling constant (λ) and the logarithmically averaged phonon frequency ω_{ln} are obtained from the following equations:

$$\lambda = 2\int_0^\infty \frac{\alpha^2 F(\omega)}{\omega} d\omega. \tag{4}$$

and

$$\omega_{ln} = exp\left(2\lambda^{-1}\int_0^\infty \frac{d\omega}{\omega}\alpha^2 F(\omega) ln\omega\right). \tag{5}$$

Then, the Allen-Dynes modified McMillan equation [71,72] is usually utilized to procure the superconducting transition temperature T_c:

$$T_c = \frac{\omega_{\ln}}{1.2}\exp\left(-\frac{1.04(1+\lambda)}{\lambda - \mu^*(1+0.62\lambda)}\right), \tag{6}$$

where μ^* is the Coulomb pseudopotential representing Coulomb repulsion. The value of μ^* generally lies between 0.10 and 0.16. The average value of 0.13 is utilized for the calculation of T_c. Furthermore, the values of λ and $N(E_F)$ allow us to obtain the electronic specific heat coefficient γ, given as

$$\gamma = \frac{1}{3}\pi^2 k_B^2 N(E_F)(1+\lambda). \tag{7}$$

Finally, we have to emphasize that a denser 24×24×24 $\boldsymbol{k}$-point grid is chosen for evaluating accurate results for the electron-phonon interaction matrix.

3 Results

3.1 Structural and Electronic Properties

The orthorhombic phase of Mo_2C adopts the ζ-Fe_2N-type crystal structure with space group P_{bcn} and four formula units per primitive unit cell. Figure 1 illustrates this structure. The atoms occupy the Wyckoff positions 8(d) (x_{Mo}, y_{Mo}, z_{Mo}) for Mo and 4(c) (0, y_C, 1/4) for C, where x_{Mo}, y_{Mo}, z_{Mo} and y_C denote the internal free coordinates. Thus, this structure is formed by three lattice parameters, a, b and c, and four internal structural parameters, x_{Mo}, y_{Mo}, z_{Mo} and y_C. As can be seen from Fig. 1, the primitive unit cell of orthorhombic Mo_2C includes twelve atoms, which are eight molybdenum and four carbon atoms. The carbon atoms in orthorhombic Mo_2C regulate themselves in such way that each molybdenum atom possesses three almost planar carbon neighbors while each carbon atom coordinates with six molybdenum atoms.

We first optimized the structure under the minimum conditions of the total energy and the forces acting on the atoms. Then, the values of bulk modulus (B) and its pressure derivative ($B^{'}$) were obtained by minimizing the crystal total energy for different values of the crystal volume by means of the Murnaghan equation of state [73]. The calculated values of the lattice parameters (a, b and c), the internal free coordinates (x_{Mo}, y_{Mo}, z_{Mo} and y_C), the bulk modulus (B) and its pressure derivative ($B^{'}$), and their comparison with available experimental [13–16,18] and theoretical results [20,44,46–57] are presented in Tab. 1. Generally speaking, the calculated structural parameters accord well with their experimental [13–16,18] and previous theoretical [20,44,46–57] values. In particular, each lattice parameter differs from its experimental value by less than 2%. The values of bond-lengths between each Mo atom and its three neighboring C atoms are found to be 2.115 $\mathring{A}$, 2.122 $\mathring{A}$ and 2.139 $\mathring{A}$ which are all shorter than the sum of the covalent radii for Mo+C of 2.220 $\mathring{A}$. This result reveals that a strong covalent Mo-C interaction is present in the orthorhombic Mo_2C but some ionic character in this superconductor exists due to the difference in the electronegativity among the comprising elements.

Fig. 2 (a) displays the calculated electronic band structure of Mo_2C along the high symmetry directions in the Brillouin zone of simple orthorhombic lattice. The gross features of calculated band structure are consistent with those reported in previous theoretical calculations [50,53]. The calculated band structure reveals that the orthorhombic Mo_2C is a three-dimensional metal because several bands with large dispersion cross the Fermi level along several symmetry directions. The bonding in this material can be categorized as an interplay between covalent, metallic, and ionic characters. In order to understand the character of electronic bands the total and partial density of states (DOS) are depicted in Fig. 2 (b). The presence of a gap of 4.1 eV divides the valence DOS into two obvious regions. The first region, lying from -13.4 eV to -11.2 eV, originates from C 2s states with smaller but considerable contributions from the 4d and 5p states of Mo atoms. Mo 4d and C 2p states display strong hybridization with each other in the lower part of the second region extending from -7.1 to -4.0 eV, confirming strong Mo-C covalent bonding. The remaining part of the second valence region reveals a dominance of Mo 4d states with much lesser contributions from other electronic states. This picture indicates that the metallic nature of orthorhombic Mo_2C arises mainly from Mo atoms. Since Cooper pairs in the BCS theory are created by electrons having energies close to the Fermi level, the DOS in the vicinity of the Fermi level must be examined in detail. The DOS at the Fermi level ($N(E_F)$) has a value of 6.657 States/eV which coincides nicely with its previous GGA value of 6.546 States/eV [50]. The contributions of Mo and C atoms to the value of $N(E_F)$ amount to 0.6124 States/eV (94%) and 0.0533 States/eV (6%), respectively. In particular, Mo 4d states alone contribute to the value of $N(E_F)$ up to approximately 92%. This huge contribution suggests that Mo 4d electrons play a main role in the formation of superconducting state for the orthorhombic Mo_2C since the large value of $N(E_F)$ leads to an enhancement in the value of λ according to the McMillan-Hopfield expression [72];

$$\lambda = \frac{N(E_F) < I^2 >}{M < \omega^2 >}, \tag{8}$$

where $< \omega^2 >$ depicts the average of squared phonon frequencies, M is the average atomic mass, and $< I^2 >$ denotes the Fermi surface average of squared electron-phonon coupling interaction. This expression obviously reveals that the value of λ increases linearly with increasing value

of $N(E_F)$. Thus, it can be concluded that the d electrons of Mo atoms are essential for the superconducting properties of orthorhombic Mo_2C.

The first Brillouin zone and Fermi surfaces of the simple orthorhombic Mo_2C are presented in Fig. 3. Our calculations suggest that there are eight different Fermi surface sheets for this compound. Between Fig. 3(b) and Fig. 3(c), these eight sheets are divided equally and both figures present four Fermi sheets for a better aspect. [Huseyin, I have changed 'Fermi surfaces' to 'Fermi surface sheets'.] The zone center nesting has a simple sphere-like shape, corresponding to the electronic bands near the Γ high symmetry point being isotropic. Similar nesting occurs near the R high symmetry point. As can be seen from the Fig. 2, there are no bands crossing the E_F along the X-S direction, thus there is no nesting along this direction. Along the Γ-R direction, there are four hole pockets and one electron pocket, with 2-fold degenerated bands constituting Fermi surfaces. The same bands are degenerated into 4-fold bands along the R-T direction and three hole pockets and one electron pocket Fermi surfaces appear in this direction. The 4d electrons of the Mo atoms domination over the E_F and valence bands lead a resonance in the DOS, and two complex Fermi surface curves are shaped which can be seen in both Fig. 3(b) and Fig. 3(c). [Huseyin, I did not understant this sentence. Please could you make a clearer statement.]

3.2 Elastic and Mechanical Properties

The mechanical performance of orthorhombic Mo_2C plays a substantial role for the application as wear resistance material. Therefore, it is mandatory to analyze its elastic properties to construe its mechanical properties. For an orthorhombic system, there are nine independent elastic constants which are C_{11}, C_{12}, C_{13}, C_{22}, C_{23}, C_{33}, C_{44}, C_{55} and C_{66}. The effective stress-strain approach [60], based on the generalized Hooke's law, has been employed to calculate these nine independent elastic constants. Their calculated values are presented in Tab.2 together with previous GGA results [50,55,57] for comparison. Our calculated results are coherent with previous GGA results [50,55,57]. The mechanical stability criterions [74] for an orthorhombic system can be expressed as:

$$C_{ii} > 0 \quad (i = 1, 6), \qquad C_{11} + C_{22} - 2C_{12} > 0, \tag{9}$$

$$C_{22} + C_{33} - 2C_{23} > 0, \qquad C_{11} + C_{33} - 2C_{13} > 0 \tag{10}$$

$$C_{11} + C_{22} + C_{33} + 2C_{12} + 2C_{13} + 2C_{23} > 0. \tag{11}$$

The calculated values of the second order elastic constants meet the above criterions, revealing the mechanical stability of Mo_2C in its orthorhombic ζ-Fe_2N-type crystal structure.

The nine independent single crystal elastic constants of orthorhombic Mo_2C can be utilized to derive its mechanical properties such as bulk modulus (B), shear modulus (G), Young's modulus (E) and Poisson's ratio (σ). Frequently, the values of B and G, are evaluated by using Voigt [61] and Reuss [62] approximations, in which the first one [61] corresponds to uniform strain throughout a polycrystal, which are given by the following equations:

$$B_V = \frac{1}{9}(C_{11} + C_{22} + C_{33} + 2C_{12} + 2C_{13} + 2C_{23}), \tag{12}$$

$$G_V = \frac{1}{15}(C_{11} + C_{22} + C_{33} + 3C_{44} + 3C_{55} + 3C_{66} - C_{12} - C_{13} - C_{23}). \tag{13}$$

The second approximation [62] considers a uniform stress and provides the values of B and G as functions of elastic compliance constants ($S_{ij} = C_{ij}^{-1}$):

$$B_R = \frac{1}{(S_{11} + S_{22} + S_{33}) + 2(S_{12} + S_{13} + S_{23})}, \tag{14}$$

$$G_R = \frac{15}{4(S_{11} + S_{22} + S_{33}) - 4(S_{12} + S_{13} + S_{23}) + 3(S_{44} + S_{55} + S_{66})}. \tag{15}$$

The arithmetic average of Voigt [61] and Reuss [62] approximations is known as the Hill approximation [63] in the literature. According to this approximation [63], the values of bulk modulus and shear modulus equal to $B_H = \frac{B_V + B_R}{2}$ and $G_H = \frac{G_V + G_R}{2}$, respectively. Finally, the values of Young's modulus (E) and Poisson's ratio (σ) are estimated by using the following equations:

$$E = \frac{9B_H G_H}{3B_H + G_H}, \quad \sigma = \frac{(3B_H - 2G_H)}{(6B_H + 2G_H)}. \tag{16}$$

The estimated values of the isotropic bulk modulus B_H, shear modulus G_H, Young's modulus E, B_H/G_H ratio and Poisson's ratio for orthorhombic Mo_2C are presented in Tab. 3, along with available experimental [45] and previous GGA [50,55,57] results. The calculated values of E, G_H, B_H, B_H/G_H and σ are analogous with their corresponding experimental values [45] as well as their previous GGA values [50,55,57]. The value of Poisson's ratio can be utilized to designate the brittleness and ductility of the materials [75]. If this ratio is greater than the critical value of 0.26, the material exhibits ductile behavior; otherwise, it exhibits brittle behavior. As can be seen from Tab. 3, the Poisson's ratio of Mo_2C has a value of 0.292, suggesting that this superconductor acts in a ductile manner. Furthermore, Pugh's ratio [76] (B_H/G_H) is another index which defines the ductile and brittle nature of materials. If this ratio is greater that its critical value of 1.75, the materials behaves in a ductile manner; otherwise, it behaves in a brittle manner. The value of Pugh's ratio for orthorhombic Mo_2C is 2.067, confirming its ductile nature. Furthermore, the value of Cauchy pressure (C_{12}-C_{12}) can be also used to defines the ductile and brittle nature of materials. A negative value of this pressure suggests a brittle character while its positive value means a ductile behavior [77]. The calculated value of Cauchy pressure for orthorhombic Mo_2C is 88.1 GPa, strongly confirming the ductile nature of this superconductor.

It is well known that the considerable elastic anisotropy may cause microcracks in materials [78]. Therefore, the elastic anisotropy is an essential quantity to improve their durability. Several anisotropic indexes exist in the literature but we have used the universal anisotropic index (A^U) and the percent of anistropy indexes (A_B and A_G) which are given by the following equations:

$$A^U = 5\frac{G_V}{G_R} + \frac{B_V}{B_R} - 6 \geq 0 \tag{17}$$

$$A_B = \frac{B_V - B_R}{B_V + B_R} \tag{18}$$

$$A_G = \frac{G_V - G_R}{G_V + G_R}. \tag{19}$$

$$\tag{20}$$

The calculated values of A^U, A_B, A_G and their comparison with previous GGA results [50,55,57] are summarized in Tab. 3. In general, our calculated values coincide with previous GGA results [50,55,57]. If the values of A^U, A_B and A_G equal to zero, the material exhibits an isotropic character. The large variation from zero signals the anisotropic character of material. As can be seen from Tab. 3, the value of A_B for orthorhombic Mo_2C is considerably small, revealing that this superconductor exhibits a weak anisotropic character in bulk modulus. The value of A_G is significantly larger than that of A_B which signals a considerable difference in the values of G_V and G_R. This difference will affect the value of A^U which is a much better pointer for mechanical anisotropic properties. The value of this index is found to be 0.1452 for orthorhombic Mo_2C which remarks its anisotropic character.

As an essential quantity, the Debye temperature (Θ_D) is connected with many physical properties of solids, such as specific heat, elastic constants, and melting temperature. At low temperatures the vibrational excitations originates merely from acoustic branches. Therefore, the calculated value of Θ_D from the second order elastic constants is frequently coherent with its determined value from specific heat measurements. As a consequence, the derived values of B_H and G_H from the second order elastic constants can be utilized to estimate transverse (V_T), longitudinal (V_L) and mean sound (V_M) elastic wave velocities using the following equations:

$$V_T = \left(\frac{G_H}{\rho}\right)^{1/2} \tag{21}$$

$$V_L = \left(\frac{3B_H + 4G_H}{3\rho}\right)^{1/2} \tag{22}$$

$$V_m = \left[\frac{1}{3}\left(\frac{2}{V_T^3} + \frac{1}{V_L^3}\right)\right]^{-1/3}, \tag{23}$$

$$\tag{24}$$

where ρ is the mass density of the material. The calculated value of V_M allow us to derive the value of Θ_D from the following equation [79]:

$$\Theta_D = \frac{h}{k_B}\left(\frac{3n}{4\pi}\frac{N_A\rho}{M}\right)^{1/3} V_m. \tag{25}$$

Here h, k_B, N_A, M and n refer to Planck's constant, Boltzmann constant, Avagadro's number, the molecular weight and the number of atoms in the molecule, respectively. The calculated values of V_T, V_L and V_M and Θ_D and their comparison with existing experimental [45] and theoretical [50,55,57] results are summarized in Tab. 4. This table clearly reveals that the calculated values of these physical parameters are comparable with their corresponding experimental [45] and theoretical [50,55,57] values.

3.3 Phonon and Electron-Phonon Interaction Properties

We first probe the zone-centre phonon modes of orthorhombic Mo_2C categorized by the irreducible representations of the point group D_{2h}(mmm). As predicted from group theory, the symmetries of the zone-centre optical phonon modes can be expressed as

$$\Gamma(D_{2h}(mmm)) = 4A_g \oplus 5B_{2g} \oplus 5B_{1g} \oplus 4B_{1u} \oplus 4B_{2u} \oplus 4A_u \oplus 4B_{3g} \oplus 3B_{3u}.$$

The calculated zone-centre phonon frequencies, their electron-phonon coupling parameters and the dominant ions in contribution to the eigenvectors of the vibrational phonon modes are presented in Tab. 5. Our electron-phonon calculations reveal that the majority of the phonon modes possess a very small electron-phonon coupling parameter except for the lowest A_g, the second A_g and the lowest B_{3g} phonon modes. The eigenvector representations of these phonon modes are displayed in Fig. 4. As it is expected, these phonon modes are mainly dominated by the motion of Mo atoms because of the significant existence of Mo d states at the Fermi energy. As can be seen from Fig. 4, eigenvector representations of these phonon modes modulate the bond angles in the orthorhombic phase of Mo_2C which leads to the overlap of Mo and C electronic states. As a consequence, these phonon branches have larger electron-phonon coupling parameters than the remaining phonon modes.

Up to now, we have only analyzed the zone-centre phonon modes. However, full understanding and a trustworthy calculation of the electron-phonon coupling needs the knowledge of the complete phonon spectrum throughout the Brillouin zone. Thus, the calculated phonon spectrum of orthorhombic Mo_2C along high symmetry directions in the first Brillouin zone of simple orthorhombic lattice is shown in Fig. 5 (a). Our calculated phonon spectrum looks similar to the one presented in the theoretical work of Connetable [57]. No imaginary phonon modes are present in the phonon spectrum of orthorhombic Mo_2C, revealing the dynamical stability of this compound in its ζ-Fe_2N-type crystal structure. This phonon spectrum splits in two apparent regions: low frequency region (LFR) (0-9.5 THz) and high frequency region (HFR) (18-21 THz) which are separated between each other by a large phonon band gap of 8.5 THz, arising from the huge mass difference between Mo and C atoms. The LFR is composed of three acoustic and twenty one optical phonon branches. The acoustic phonon branches in this region disperse up to 5 THz which leads to a strong overlap between them and the low-lying optical phonon branches. The HFR is formed by twelve optical phonon branches. The nature of all phonon branches can be understood more obviously by presenting the total and partial density of states in Fig. 5 (b). As it is expected, in the LFR, the main contribution to the DOS features comes from Mo atoms while the vibrations of lighter C atoms dominate the HFR. Since the low frequency phonon modes are mainly characterized by the vibrations of Mo atoms and their d states dominate the density of states at the Fermi level, Mo atoms and their d states have a potential to play an essential role in the transition from the normal state to the superconducting state for orthorhombic Mo_2C according to the McMillan-Hopfield expression (see Eq. 8).

In order to examine the strengths which different modes of ionic motion interact with the electrons at the Fermi energy, and hence are capable of influencing the superconducting properties of orthorhombic Mo_2C strongly, we have presented the Eliashberg spectral function $\alpha^2F(\omega)$ and the frequency variation of the average electron-phonon coupling parameter in Fig. 6. We will examine the spectral contribution to the value of average electron-phonon coupling parameter.

In frequency region from 2.9 to 5.8 THz, the value of λ increases rapidly with increment in phonon frequency. Thus, the largest subscription to λ comes from three acoustic phonon modes and low-lying optical phonon modes in this region with around 77%. This result confirms that Mo-related phonon modes couple strongly to electrons due to the remarkable existence of Mo d electrons at the Fermi level. Finally, the calculated values of the physical quantities ($N(E_F)$, ω_{ln}, λ, γ, and T_c) related to superconductivity in the orthorhombic phase of Mo_2C are presented in Tab. 6 together with available experimental [21] and theoretical [50,53] results. The value of λ amounts to 0.709, indicating that the orthorhombic phase of Mo_2C is a phonon-mediated superconductor with the intermediate electron-phonon coupling strength. The calculated value of $N(E_F)$ accords with its previous GGA values [50,53] while the calculated value of T_c is almost equal to its experimental value of 7.30 K [21]. Unfortunately, no experimental data or theoretical results exist for the values of ω_{ln} and γ. Therefore, our presented reults can provide a useful quidance for future exoerimental and theoretical works on this superconductor.

4 Summary

We have probed the structural and electronic properties of Mo_2C crystallizing in the simple orthorhombic ζ-Fe_2N-type crystal structure by using the generalized gradient approximation of the density functional theory and the plane wave *ab initio* pseudopotential method. The calculated values of three lattice parameters (a, b and c) and four internal coordinates (x_{Mo}, y_{Mo}, z_{Mo} and y_C) are compatible with their corresponding experimental values. The bonding in this material can be classified as an interplay between covalent, metallic, and ionic characters. Mo d electrons dominate the energy states near the Fermi level. The effective stress-strain approach based on the generalized Hooke's law reveals the mechanical stability of this superconductor. The calculated values of elastic constants have been used to determine the mechanical properties of orthorhombic Mo_2C such as bulk modulus (B), shear modulus (G), Young's modulus (E) and Poisson's ratio (σ) using the Voigt-Reuss-Hill (VHR) approach. The calculated values of B, G, E and σ are in good accordance with their corresponding experimental values. Furthermore, the calculated value of Pugh's ratio reveals the ductile nature of orthorhombic Mo_2C.

In addition to the structural, electronic, elastic and mechanical properties of orthorhombic Mo_2C, its vibrational properties have been analyzed by using a linear response approach. No imaginary phonon modes are presented in the calculated phonon spectrum of orthorhombic Mo_2C, revealing the dynamical stability of this superconductor in its orthorhombic ζ-Fe_2N-type crystal structure. The partial phonon DOS of orthorhombic Mo_2C depicts a dominance of Mo atoms in the low frequency region due to the heavier mass of Mo atoms as compared to that of C atoms. Since Mo atoms dominate the phonon DOS features in the low frequency phonon region and their d states dominate the states near the Fermi level, these atoms and their d states have a potential to play essential role in the transition from the normal state to the superconducting state. An analysis of the Eliashbergh spectral function reveals that the three acoustic phonon branches and low-lying optical phonon branches mainly characterized by the vibrations of Mo atoms are more involved in the process of scattering of electrons than the phonon modes with high frequency. From the integration of Eliashberg spectral function, the value of the average electron-phonon coupling parameter is determined to be 0.709, signaling the intermediate electron-phonon interaction in this superconductor. Finally, using the calculated

value of average electron-phonon coupling parameter, the value of superconducting temperature is estimated to be 7.37 K which accords excellently with its measured value of 7.30 K.

References

[1] J.G. Chen, Carbide and Nitride Overlayers on Early Transition Metal Surfaces: Preparation, Characterization, and Reactivities, Chem. Rev. 96 (1996) 1477-1498.

[2] J.G. Chen, J. Eng, and S.P. Kelty, NEXAFS determination of electronic and catalytic properties of transition metal carbides and nitrides: From single crystal surfaces to powder catalysts, Catal. Today 43 (1998) 147-158.

[3] Y. Kumashiro, Electric Refractory Materials, Marcel Dekker, New York, 2000.

[4] J.A. Nelson, M.J. Wagner, High Surface Area Mo_2C and WC Prepared by Alkalide Reduction, Chem. Mater. 14 (2002) 1639-1642.

[5] H.H.H. Wu, and J.G. Chen, Surface Chemistry of Transition Metal Carbides, Chem. Rev. 105 (2005) 185-212.

[6] L.E. Toth, Transition Metal Carbides and Nitrides, Academic Press, New York, 1971.

[7] V.A. Gubanov, A.L. Ivanovsky, V.P. Zhukov, Electronic Structure of Refractory Carbides and Nitrides, Cambridge University Press, Cambridge, 1994.

[8] M. Wiefssner, M. Leisch, H. Emminger, A. Kulmburg, Phase transformation study of a high speed steel powder by high temperature X-ray diffraction, Mater. Charact. 59 (2008) 937-943.

[9] X.H. Wang, F. Han, X.M. Liu, S.Y. Qu, Z.D. Zou, Effect of molybdenum on the microstructure and wear resistance of Fe-based hardfacing coatings, Mater. Sci. Eng. A 489 (2008) 193-200.

[10] A.S. Chaus, M. Hudakova, Wear resistance of high-speed steels and cutting performance of tool related to structural factors, Wear 267 (2009) 1051-1055.

[11] M. Pellizzari, D. Cescato, M.G. De Flora, Hot friction and wear behaviour of high speed steel and high chromium iron for rolls, Wear 267 (2009) 467-475.

[12] A. Zaoui, S. Kacimi, B. Bouhafs, A. Roula,First-principles study of bonding mechanisms in the series of Ti, V, Cr, Mo, and their carbides and nitrides, Physica B 358 (2005) 63-71.

[13] E. Parthe, V. Sadagopan, The structure of dimolybdenum carbide by neutron diffraction techniqueThe structure of dimolybdenum carbide by neutron diffraction technique, Acta Cryst. 16 (1963) 202-205.

[14] A. N. Christensen, A neutron diffraction investigation on a crystal of α-M_2C, Acta Chemica Scandinavica A 31 (1977) 509-511.

[15] T. Epicier, J.Dubois, C. Esnouf, G. Fantozzi, P. Convert, Neutron powder diffraction studies of transition metal hemicarbides M_2C_{1-x}–II. In situ high temperature study on W_2C_{1-x} and Mo_2C_{1-x}, Acta Metallurgica 36 (1988) 1903-1921.

[16] S. Otani, Y. Ishizawa, Preparation of Mo_2C single crystals by the floating zone method, J. Cryst. Growth 154 (1995) 202-204.

[17] P. Liu, J.A. Rodriguez, Effects of carbon on the stability and chemical performance of transition metal carbides: A density functional study, J. Chem. Phys. 120 (2004) 5414-5423.

[18] K.M. Reddy, T.N. Rao, J. Revathi, and J. Joardar, Structural stability of α/β-Mo_2C during thermochemical processing, J. Alloys Compd. 494 (2010) 386–391.

[19] K. Page, J. Li, R. Savinelli, H.N. Szumila, J. Zhang, J.K. Stalick, T. Proffen, S.L. Scott and R. Seshadri, Reciprocal-space and real-space neutron investigation of nanostructured Mo_2C and WC, Surf. Sci. 10 (2008) 1499–1510.

[20] J. Haines, J.M. Leger, C. Chateau and J.E. Lowther, Experimental and theoretical investigation of Mo_2C at high pressure, J. Phys.: Condens. Matter. 13 (2001) 2447–2454.

[21] N. Morton, B.W. James, G.H. Wostenholm, D.G. Pomfret, M.R. Davies, J.L. Dykins, Superconductivity of molybdenum and tungsten carbides, Journal of the Less Common Metals 25 (1971) 97-106.

[22] J.S. Lee , M.H. Yeom, K.Y. Park, I.-S. Nam, J.S. Chung, Y.G. Kim, S.H. Moon, H. Sang Preparation and benzene hydrogenation activity of supported molybdenum carbide catalysts, J. Catal. 128 (1991) 126–136.

[23] S.T. Oyama,Preparation and catalytic properties of transition metal carbides and nitrides, Catal. Today 15 (1992) 179-200.

[24] C. Marquez-Alvarez, J.B. Calridge, A.P.E. York, J. Sloan, M.L.H. Green,Benzene hydrogenation over transition metal carbides, Studies in surface science and catalysis, 106 (1997) 485–490.

[25] M.K. Neylon, S. Choi, H. Kwon, K.E. Curry, L.T. Thompson, Catalytic properties of early transition metal nitrides and carbides: n-butane hydrogenolysis, dehydrogenation and isomerization, Appl. Catal. A 183 (1999) 253–263.

[26] J. Du, J. Wu, T. Guo, R. Zhao, J. Li, Catalytic performance of Mo_2C supported on onion-like carbon for dehydrogenation of cyclohexane, RSC Adv. 4 (2014) 53950-53953.

[27] G. S. Ranhotra, A. T. Bell, J. A. Reimer, Catalysis over molybdenum carbides and nitrides: II. Studies of CO hydrogenation and C_2H_6 hydrogenolysis, J. Catal. 108 (1987) 40-49.

[28] S. S. Y. Lin, W. J. Thomson, T. J. Hagensen, S. Y. Ha, Steam reforming of methanol using supported Mo_2C catalysts. Appl Catal A Gen 318 (2007) 121–127. methanation.

[29] F. Solymosi, J. Cserenyi, A. Szke, T. Bansagi, A. Qszko, Aromatization of methane over supported and unsupported Mo-based catalysts, J. Catal. 165 (1997) 150-161.

[30] K. Oshikawa, M. Nagai, S. Omi, Characterization of molybdenum carbides for methane reforming by TPR, XRD, and XPS, J. Phys. Chem. B 105 (2001) 9124-9131.

[31] R. Barthos, T. Bansagi, T. S. Zakar, F. Solymosi, Aromatization of methanol and methylation of benzene over Mo_2C/ZSM-5 catalysts, J. Catal. 247 (2007) 368-378.

[32] S. J. Ardakani, K.J. Smith, A comparative study of ring opening of naphthalene, tetralin and decalin over Mo_2C/HY and Pd/ HY catalysts. Appl Catal A Gen 403 (2011) 36–47.

[33] K.R. McCrea, J.W. Logan, T.L. Tarbuck, J.L. Heiser, M.E. Bussell, Thiophene hydrodesulfurization over alumina-supported molybdenum carbide and nitride catalysts: Effect of Mo loading and phase, J. Catal. 171 (1997) 255-267.

[34] P.D. Costa, C. Potvin, J. M. Manoli, J. L. Lemberton, G. Prot, G. D. Mariadassou, New catalysts for deep hydrotreatment of diesel fuel: Kinetics of 4, 6-dimethyldibenzothiophene hydrodesulfurization over alumina-supported molybdenum carbide, J. Mol. Catal. A: Chem. 184 (2002) 323-333.

[35] V. Sundaramurthy, A. K. Dalai, J. Adjaye, HDN and HDS of different gas oils derived from Athabasca bitumen over phosphorus-doped NiMo/γ-Al_2O_3 carbides, J. Appl. Catal. B: Environ. 68 (2006) 38-48.

[36] J.C. Schlatter, S.T. Oyama, J.E. Metcalfe, J.M. Lambert, Catalytic behavior of selected transition metal carbides, nitrides, and borides in the hydrodenitrogenation of quinoline, Ind. Eng. Chem. Res. 27 (1988) 1648-1653.

[37] V. Schwartz, S. T. Oyama, Reaction network of pyridine hydrodenitrogenation over carbide and sulfide catalysts, J. Mol. Catal. A: Chem. 163 (2000) 269-282.

[38] R. Barthos, F. Solymosi, Hydrogen production in the decomposition and steam reforming of methanol on Mo_2C/carbon catalysts, F. J. Catal. 249 (2007) 289-299.

[39] P. Liu and J. A. Rodriguez, Water-gas-shift reaction on molybdenum carbide surfaces: essential role of the oxycarbide, J. Phys. Chem. B 110 (2006) 19418–19425.

[40] M. Nagai, K. Matsuda, Low-temperature water-gas shift reaction over cobalt-molybdenum carbide catalyst, J. Catal. 238 (2006) 489-496.

[41] J. A. Schaidle, A. C. Lausche, L. T. J. Thompson, Effects of sulfur on Mo_2C and Pt/Mo_2C catalysts: Water gas shift reaction, Catal. 272 (2010) 235-245.

[42] N. M. Schweitzer, J. A. Schaidle, O. K. Ezekoye, X. Pan, S. Linic and L. T. Thompson, High activity carbide supported catalysts for water gas shift, J. Am. Chem. Soc. 133 (2011) 2378–2381.

[43] A. S. Rocha, A. B. Rocha and V. T. da Silva, Benzene adsorption on Mo_2C: A theoretical and experimental study, Appl. Catal. A 379 (2010) 54–60.

[44] A. Vojvodic, Steam reforming on transition-metal carbides from density-functional theory, Catal. Lett. 142 (2012) 728–735.

[45] M. Cankurtaran, S.P. Dodd, B. James, Ultrasonic study of the temperature and pressure dependences of the elastic properties of ceramic dimolybdenum carbide (α-Mo_2C), J. Mater. Sci. 39 (2004) 1241–1248.

[46] H. W. Hugosson, O. Eriksson, U. Jansson, B. Johansson, Phase stabilities and homogeneity ranges in 4 d-transition-metal carbides: A theoretical study, Phys. Rev. B 63 (2001) 134108.

[47] J. Ren, C-F. Huo,J. Wang, Y-W. Li, H. Jiao, Surface structure and energetics of oxygen and CO adsorption on α-Mo_2C (0001), Surface Science 596 (2005) 212–221.

[48] C. Pistonesi, A. Juan, A.P. Farkas, F. Solymosi, DFT study of methanol adsorption and dissociation on β-Mo_2C (001), Surface Science 602 (2008) 2206–2211.

[49] X.R. Wang, M.F. Yan, and H.T. Chen, First-principle calculations of hardness and melting point of Mo_2C, J. Mater. Sci. Technol. 25 (2009) 419–422.

[50] H.L. Liu, J.C. Zhu, Z.H. Lai, R.D. Zhao, D. He, A first-principles study on structural and electronic properties of Mo_2C, Scripta Mater. 60 (2009) 949–952.

[51] A. J. Medford, A. Vojvodic, F. Studt, F. Abild-Pedersen and J. K. Nrskov, Elementary steps of syngas reactions on Mo_2C (001): Adsorption thermochemistry and bond dissociation, J. Catal. 290 (2012) 108–1176.

[52] F.Z. Abderrahim , H.I. Faraoun, T. Ouahrani, Structure, bonding and stability of semi-carbides M_2C and sub-carbides M_4C (M= V, Cr, Nb, Mo, Ta, W): A first principles investigation, Physica B 407 (2012) 3833–3838.

[53] J. R. S. Politi, F. Vines, J. A. Rodriguez, F. Illas, Atomic and electronic structure of molybdenum carbide phases: bulk and low Miller-index surfaces, Phys. Chem. Chem. Phys. 15 (2013) 12617–12625.

[54] C. Oliveira, D. R. Salahub, H. A. de Abreu, and H. A. Duarte, Native defects in α-Mo_2C: insights from first-principles calculations, J. Phys. Chem. 118 (2014) 25517–25524.

[55] Y.Z. Liu, Y.H. Jiang, R. Zhou, X.F. Liu, J. Feng, Elastic and thermodynamic properties of Mo_2C polymorphs from first principles calculations, Ceram. Int. 41 (2015) 5239–5246.

[56] T. Wang, X. Tian, Y. Yang, Y-W. Li, J. Wang, M. Beller, H. Jiao, Surface morphology of orthorhombic Mo_2C catalyst and high coverage hydrogen adsorption, Surface Science 65 (2016) 195–202.

[57] D. Connetable, First-principles study of transition metal carbides, Mater. Res. Express 3 (2016) 126502.

[58] P. Giannozzi, S. Baroni, N. Bonini, M. Calandra, R. Car, C. Cavazzoni, D. Ceresoli, G. L. Chiarotti, M. Cococcioni, I. Dabo, A. Dal Corso, S. de Gironcoli, S. Fabris, G. Fratesi, R. Gebauer, U. Gerstmann, C. Gougoussis, A. Kokalj, M. Lazzeri, L. Martin-Samos, N. Marzari, F. Mauri, R. Mazzarello, S. Paolini, A. Pasquarello, L. Paulatto, C. Sbraccia, S. Scandolo, G. Sclauzero, A. P. Seitsonen, A. Smogunov, P. Umari, R. M. Wentzcovitch, QUANTUM ESPRESSO: a modular and open-source software project for quantum simulations of materials, J. Phys.: Condens. Matter 21 (2009) 395502.

[59] P. Giannozzi, O. Andreussi, T. Brumme, O. Bunau, M. Buongiorno Nardelli, M. Calandra, R. Car, C. Cavazzoni, D. Ceresoli, M. Cococcioni, N. Colonna, I. Carnimeo, A. Dal Corso, S. de Gironcoli, P. Delugas, R. A. DiStasio Jr., A. Ferretti, A. Floris, G. Fratesi, G. Fugallo, R. Gebauer, U. Gerstmann, F. Giustino, T. Gorni, J. Jia, M. Kawamura, H.-Y. Ko, A. Kokalj, E. Kkbenli, M. Lazzeri, M. Marsili, N. Marzari, F. Mauri, N. L. Nguyen, H.-V. Nguyen, A. Otero-de-la-Roza, L. Paulatto, S. Ponc, D. Rocca, R. Sabatini, B. Santra, M. Schlipf, A. P. Seitsonen, A. Smogunov, I. Timrov, T. Thonhauser, P. Umari, N. Vast, X. Wu, and S. Baroni, Advanced capabilities for materials modelling with Quantum ESPRESSO, J. Phy.: Condensed Matter 29 (2017) 465901.

[60] O. Beckstein, J. E. Klepeis, G. L. W. Hart, O. Pankratov, First-principles elastic constants and electronic structure of α-Pt_2Si and PtSi, Phys. Rev. B 63 (2001) 134112.

[61] W. Voigt, Lehrbuch der Kristallphysik, Leipzig, Taubner, (1928).

[62] A. Reuss, Berechnung der Fliegrenze von Mischkristallen auf Grund der Plastizittsbedingung fr Einkristalle, Z. Angew. Math. Mech. 9 (1929) 49–58.

[63] R. Hill, The elastic behaviour of a crystalline aggregate, Proceedings of the Physical Society. Section A 65 (1952) 349-354.

[64] A.B. Migdal, Interaction between electrons and lattice vibrations in a normal metal, Sov. Phys. JETP 34 (1958) 996–1001.

[65] G.M. Eliashberg, Interactions between electrons and lattice vibrations in a superconductor, Sov. Phys. JETP 11 (1960) 696–702.

[66] R. Stumpf, X. Gonze and M. Scheffler, A List of Separable, Norm-conserving, Ab Initio Pseudopotentials, Fritz-Haber-Institut, Berlin, 1990.

[67] J.P. Perdew, K. Burke, M. Ernzerhof, Generalized gradient approximation made simple, Phys. Rev. Lett. 77 (1996) 3865–3868.

[68] T.H. Fischer, J. Almlof, General methods for geometry and wave function optimization, J. Phys. Chem. 96 (1992) 9768-9774.

[69] W. Kohn, L.J. Sham, Self-consistent equations including exchange and correlation effects, Phys. Rev. 140 (1965) A1133–A1138.

[70] H.J. Monkhorst, J.D. Pack, Special points for Brillouin-zone integrations, Phys. Rev. B 13 (1976) 5188–5192.

[71] W. L. McMillian, Transition Temperature of Strong-Coupled Superconductors, Phys. Rev. B 167 (1975) 331–344.

[72] P. B. Allen and R. C. Dynes, Transition temperature of strong-coupled superconductors reanalyzed, Phys. Rev. B 12 (1975) 905–922.

[73] F. D. Murnaghan , Proc. Nat. Acad. Sci. USA 50 (1944) 697.

[74] Z.-j. Wu, E.-j. Zhao, H.-p. Xiang, X.-f. Hao, X.-j. Liu, J. Meng, Crystal structures and elastic properties of superhard IrN_2 and IrN_3 from first principles, Phys. Rev. B 76 (2007) 054115.

[75] J. Haines, J. Leger, G. Bocquillon, Synthesis and design of superhard materials, Annu. Rev. Mater. Res. 31 (2001) 1-23.

[76] S. Pugh, XCII. Relations between the elastic moduli and the plastic properties of polycrystalline pure metals, Phil. Mag. 45 (1954) 823-843.

[77] S. Ganeshan, S.L. Shang, H. Zhang, Y. Wang, M. Mantina, and Z.K. Liu, Elastic constants of binary Mg compounds from first-principles calculations, Intermetallics 17 (2009) 313–318.

[78] P. Ravindran, L. Fast, P. A. Korzhavyi, and B. Johansson, Journal of Applied Physics 84 (1998) 4891–4904.

[79] O.L. Anderson, A simplified method for calculating the Debye temperature from elastic constants, J. Phys. Chem. Solids 24 (1963) 909-917.

Table 1
The calculated values of the lattice parameters (a, b and c), internal coordinates (x_{Mo}, y_{Mo}, z_{Mo} and y_C) the bulk modulus (B) and its pressure derivative ($B^{'}$) for Mo_2C, and their comparison with previous experimental and theoretical results.

	$a(\AA)$	$b(\AA)$	$c(\AA)$	x_{Mo}	y_{Mo}	z_{Mo}	y_C	B(GPa)	$B^{'}$
Mo_2C	4.75	6.09	5.26	0.2444	0.3785	0.0794	0.1230	299.4	4.49
Experimental [13]	4.72	6.00	5.19						
Experimental [14]	4.73	6.04	5.20	0.2450	0.3750	0.0833	0.1250		
Experimental [15]	4.74	6.03	5.21						
Experimental [16]	4.73	6.03	5.20						
Experimental [18]	4.75	6.02	5.21						
LDA [20]	4.74	6.13	5.26					307.0	4.34
GGA [44]	4.83	6.16	5.30						
LDA [46]	4.71	5.99	5.19						
GGA [47]	4.75	6.03	5.20						
GGA [48]	4.78	6.03	5.27					307.1	
GGA [49]	4.71	6.04	5.25						
GGA [50]	4.74	6.04	5.21						
GGA [51]	4.84	6.17	5.32					282.3	
GGA [52]	4.79	6.03	5.21					302.35	
GGA [53]	4.74	6.06	5.22					315.5	
GGA [54]	4.79	6.12	5.31					309.1	
GGA [55]	4.79	6.01	5.21						
GGA [56]	4.75	6.07	5.24						
GGA [57]	4.76	6.08	5.24						

Table 2
The calculated values of the nine independent elastic constants for the simple orthorhombic Mo_2C and their comparison with previosu GGA results. All parameters are in GPa units.

Source	C_{11}	C_{12}	C_{13}	C_{22}	C_{23}	C_{33}	C_{44}	C_{55}	C_{66}
Mo_2C	460.04	228.67	238.62	495.17	185.77	492.45	140.61	161.81	183.25
GGA [50]	460.49	210.88	205.78	482.74	166.95	489.39	148.19	174.67	182.44
GGA [55]	430.30	214.90	217.60	494.40	164.40	485.60	145.50	161.70	178.20
GGA [57]	454.00	224.00	212.00	487.00	166.00	490.00	146.00	184.00	171.00

Table 3
The calculated values of Young's modulus (E), shear modulus (G_H), Bulk Modulus (B_H), B_H/G_H, Poisson's ratio (σ), the universal anisotropic index (A^u), and percent anisotropy (A_B, A_G) for the simple orthorhombic Mo_2C and their comparison with available experimental and theoretical results.

Source	E (GPa)	G_H (GPa)	B_H (GPa)	B_H/G_H	σ	A^u	A_B	A_G
Mo_2C	382.3	147.9	305.9	2.067	0.292	0.1452	0.0001	0.0143
Experimental [45]	351.0	139.0	248.0	1.784	0.264			
GGA [50]	396.9	156.2	288.8	1.849	0.271	0.0973	0.0001	0.0100
GGA [55]	381.7	149.1	289.3	1.940	0.280	0.1500	0.0010	0.0150
GGA [57]	391.0	153.0	292.0	1.910	0.280	0.1367	0.0002	0.0135

Table 4
The calculated values of transverse (V_T), longitudinal (V_L), average elastic wave velocities (V_M) and Debye temperature (Θ_D) for the simple orthorhombic Mo_2C and their comparison with available experimental and theoretical results.

Source	V_T (m/s)	V_L (m/s)	V_M (m/s)	Θ_D (K)
Mo_2C	4079.16	7522.23	4551.58	580.87
Experimental [45]	3905.00	6906.00	4343.00	559.00
GGA [50]	4146.34	7397.39	4614.73	593.08
GGA [55]	4058.90	7343.90	4522.40	580.30
GGA [57]				590.00

Table 5
Calculated zone-centre phonon modes (ν in THz) and their electron-phonon coupling parameters (λ) and their eigen characters for the simple orthorhombic Mo_2C. The notations of I, R, and S denote infrared active, Raman active and silent modes, respectively.

Mode	ν	λ	Eigen characters	Mode	ν	λ	Eigen characters
A_g (R)	4.041	0.130	**Mo**+C	A_g (R)	6.937	0.026	**C**+Mo
B_{2g} (R)	4.170	0.059	**Mo**+C	A_u (S)	7.546	0.006	**Mo**
B_{1g} (R)	4.266	0.073	**Mo**+C	B_{3u} (I)	7.689	0.011	**Mo**
B_{1u} (I)	4.494	0.014	**Mo**+C	B_{3g} (R)	9.469	0.015	**Mo**+C
B_{2u} (I)	4.758	0.012	**Mo**+C	B_{2g} (R)	18.263	0.007	**C**
B_{2g} (R)	4.785	0.056	**C**+Mo	B_{1g} (R)	18.319	0.009	**C**
A_u (S)	4.867	0.015	**Mo**+C	B_{1u} (I)	18.354	0.004	**C**
A_g (R)	5.254	0.118	**Mo**+C	B_{3u} (I)	18.600	0.010	**C**
B_{2u} (I)	5.259	0.014	**Mo**+C	B_{2u} (I)	18.689	0.003	**C**
B_{3g} (R)	5.272	0.107	**Mo**+C	A_g (R)	19.413	0.004	**C**
B_{3u} (I)	5.394	0.033	**Mo**+C	B_{1u} (I)	19.423	0.008	**C**
B_{3g} (R)	5.559	0.082	**Mo**+C	B_{2u} (I)	19.799	0.002	**C**
B_{1g} (R)	5.594	0.022	**Mo**+C	B_{1g} (R)	20.124	0.006	**C**
B_{1u} (I)	5.972	0.009	**Mo**+C	A_u (S)	20.171	0.002	**C**
A_u (S)	5.986	0.011	**Mo**+C	B_{3g} (R)	20.398	0.009	**C**
B_{2g} (R)	6.368	0.062	**Mo**+C	B_{2g} (R)	21.019	0.006	**C**
B_{1g} (R)	6.414	0.018	**Mo**+C				

Table 6
The calculated values of physical quantities related to superconductivity in the simple orthorhombic Mo_2C and their comparison with available experimental and theoretical results.

Source	$N(E_F)$ (States/eV)	ω_{ln} (K)	λ	$\gamma(\frac{mJ}{molK^2})$	T_c (K)
This Work	6.657	266.01	0.709	26.745	7.37
Experimental [21]					7.30
GGA [50]	6.546				
GGA [53]	5.769				

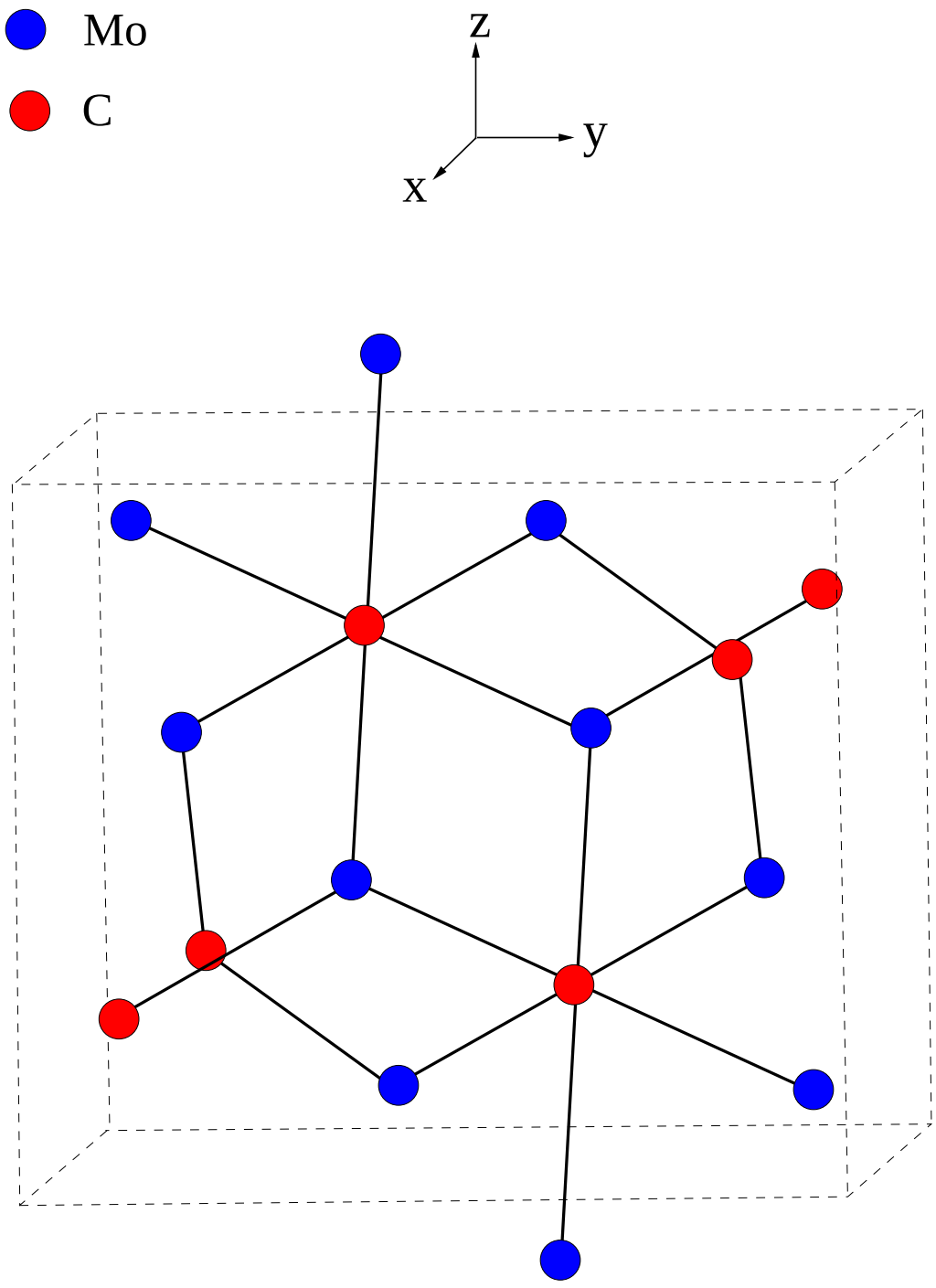

Fig. 1. (a) The simple orthorhombic ζ-Fe_2N-type crystal structure of Mo_2C superconductor.

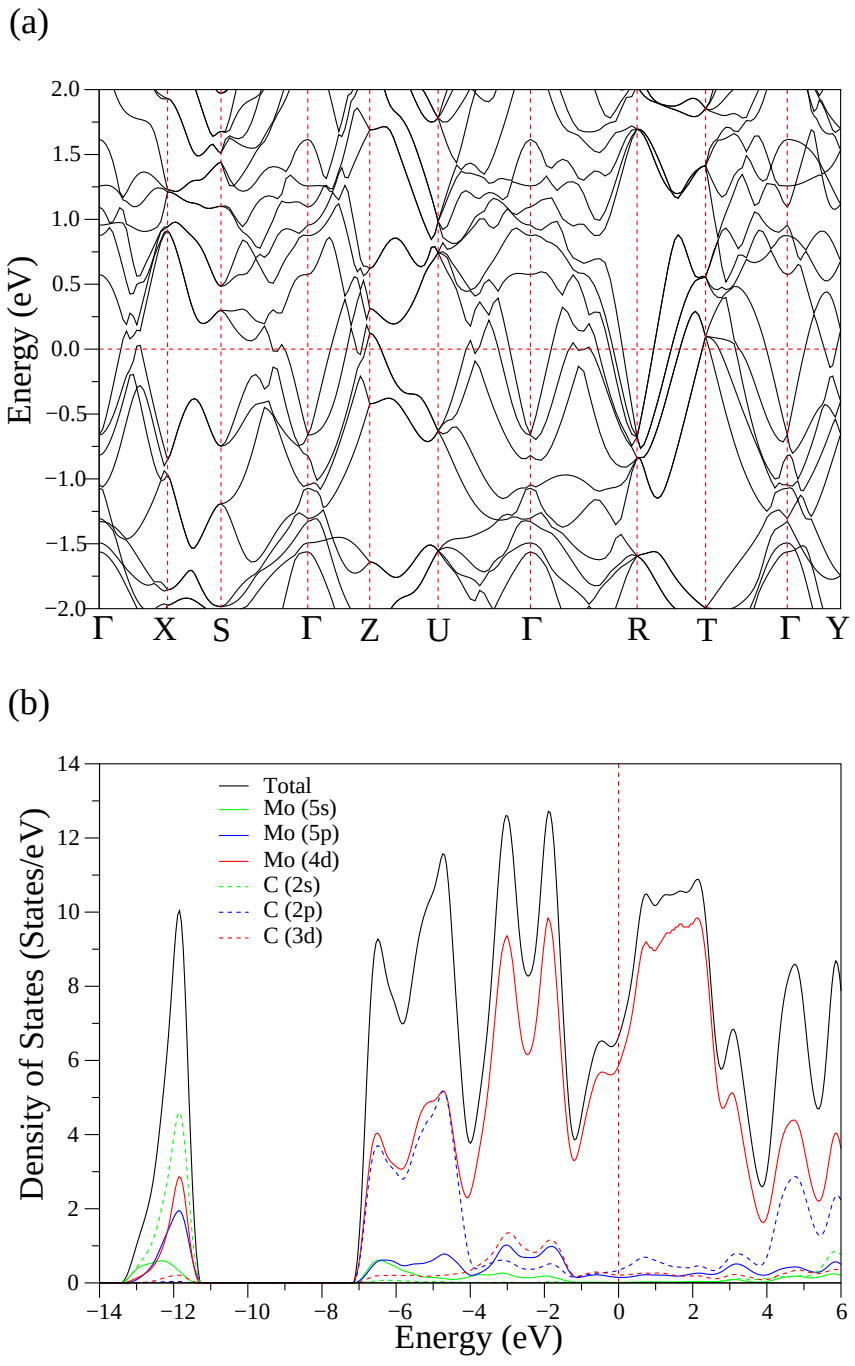

Fig. 2. (a) The electronic band structure of simple orthorhombic Mo_2C along selected symmetry directions of the simple orthorhombic Brillouin zone. The Fermi energy corresponds to 0 eV. (b) The total and atomic projected electronic local density of states for simple orthorhombic Mo_2C.

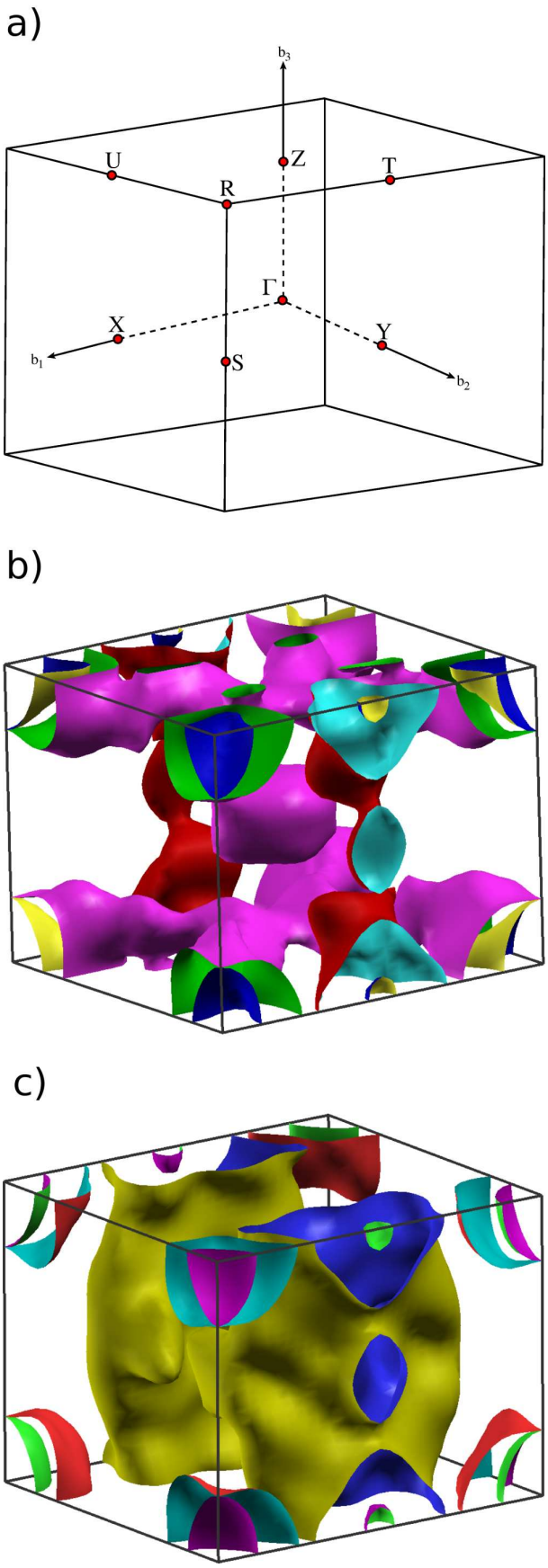

Fig. 3. Calculated Fermi Surfaces in the simple orthorhombic Mo_2C.

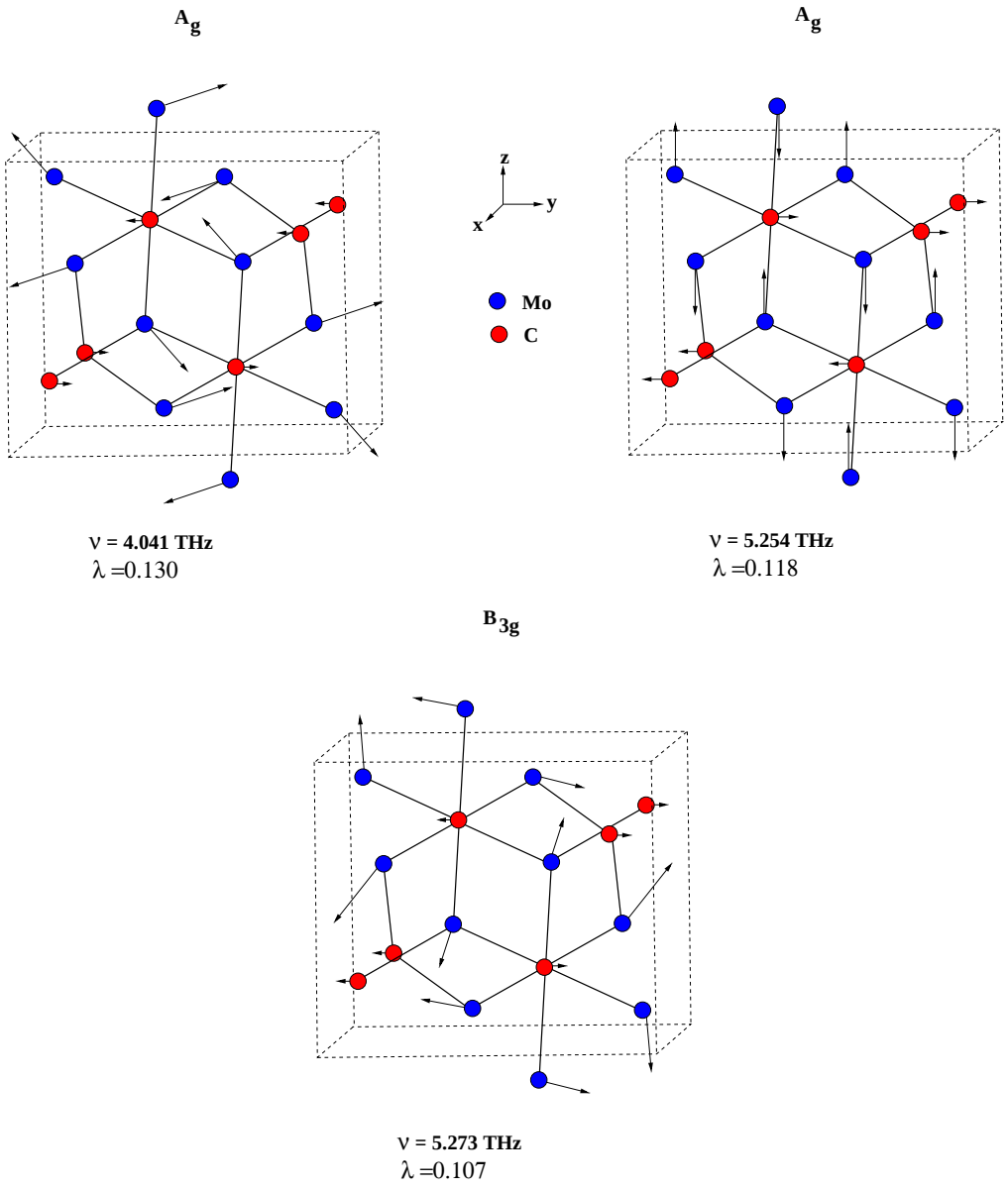

Fig. 4. Eigen atomic displacement patterns, phonon frequencies and electron-phonon coupling parameters for selected zone-center modes in the simple orthorhombic Mo_2C.

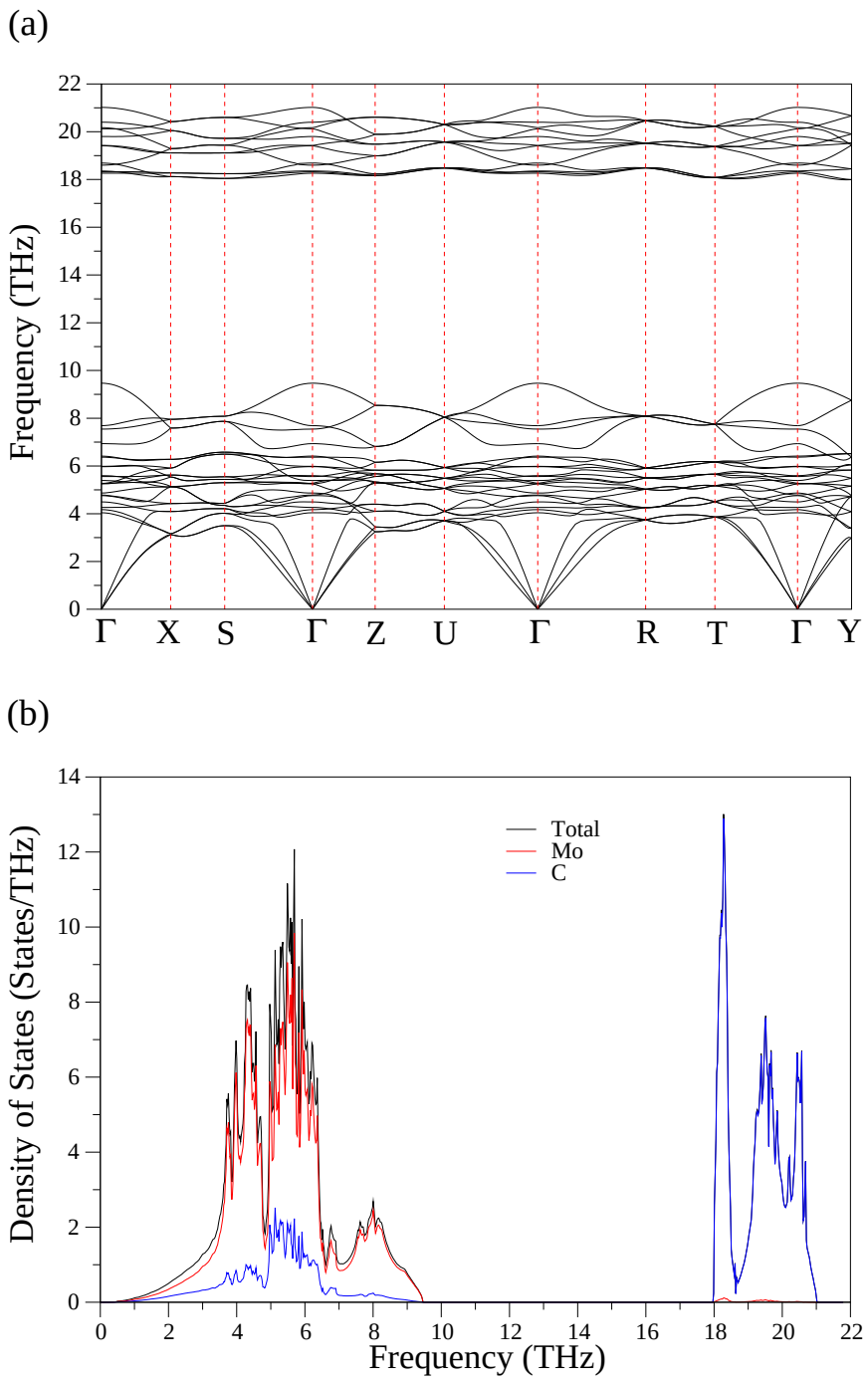

Fig. 5. The calculated phonon dispersion spectrum of simple orthorhombic Mo_2C along the high symmetry lines in the first Brillouin zone of simple orthorhombic lattice. (b) The calculated total and partial phonon density of states of simple orthorhombic Mo_2C.

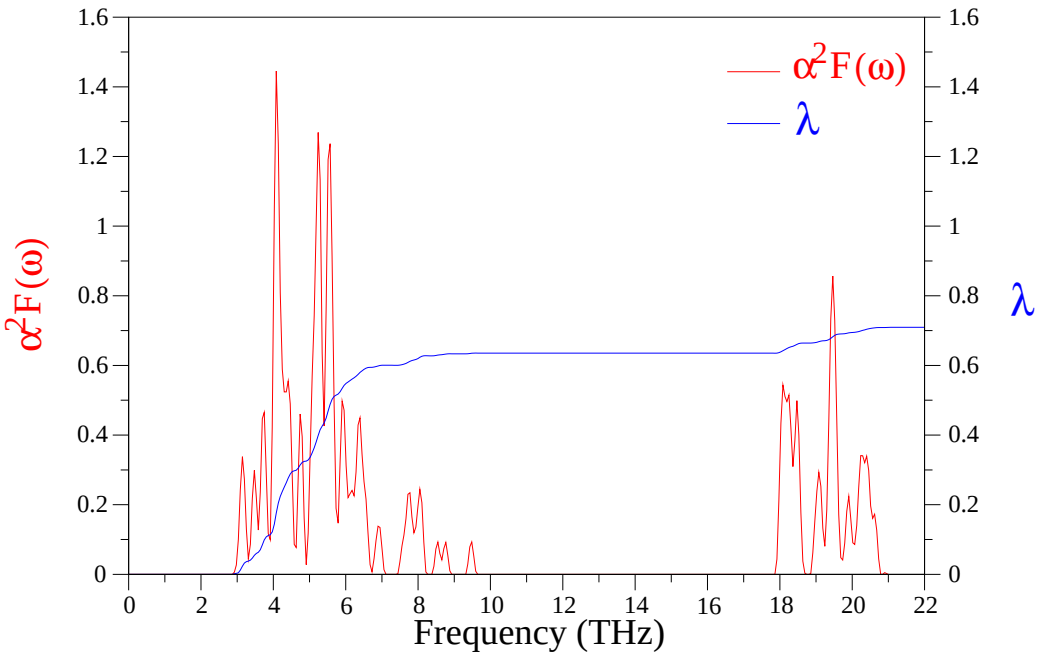

Fig. 6. Eliashberg spectral function $\alpha^2F(\omega)$ (red curve) and integrated electron-phonon coupling parameter λ (blue curve) for the simple orthorhombic Mo_2C.